

Modeling partitioning of Min proteins between daughter cells after septation in *Escherichia coli*

Supratim Sengupta^{1,2} and Andrew Rutenberg¹

¹Department of Physics & Atmospheric Science, Dalhousie University, Halifax, Nova Scotia B3H 3J5, Canada.

²Centre for Computational Biology and Bioinformatics, School of Information Technology, Jawaharlal Nehru University, New Delhi - 110 067, India.

E-mail: sengupta@mail.jnu.ac.in, andrew.rutenberg@dal.ca

Abstract. Ongoing sub-cellular oscillation of Min proteins is required to block minicelling in *E. coli*. Experimentally, Min oscillations are seen in newly divided cells and no minicells are produced. In model Min systems many daughter cells do not oscillate following septation because of unequal partitioning of Min proteins between the daughter cells. Using the 3D model of Huang *et al.*, we investigate the septation process in detail to determine the cause of the asymmetric partitioning of Min proteins between daughter cells. We find that this partitioning problem arises at certain phases of the MinD and MinE oscillations with respect to septal closure and it persists independently of parameter variation. At most 85% of the daughter cells exhibit Min oscillation following septation. Enhanced MinD binding at the static polar and dynamic septal regions, consistent with cardiolipin domains, does not substantially increase this fraction of oscillating daughters. We believe that this problem will be shared among all existing Min models and discuss possible biological mechanisms that may minimize partitioning errors of Min proteins following septation.

PACS numbers: 87.16.Ac, 87.17.Ee, 05.40.-a

Submitted to: *Phys. Biol.*

Keywords: septation, *Escherichia coli*, MinD, MinE, protein partitioning, oscillation, spatiotemporal pattern, subcellular localization, reaction diffusion, modeling.

Dated : 30 October 2018

1. Introduction

Cell division in *Escherichia coli* is initiated by the formation of a ring of the protein FtsZ on the bacterial inner membrane. This FtsZ ring shrinks [1] as the growing septum restricts the cytoplasmic channel connecting the two daughter cells. FtsZ ring formation is targeted to the mid-cell by two independent processes. Nucleoid occlusion prevents FtsZ ring formation over the nucleoids [2, 3, 4], while polar FtsZ ring formation is prevented due to the oscillatory dynamics of the Min family of proteins. The pole-to-pole oscillation of MinD and MinE [5, 6, 7] targets MinC to the polar inner membrane where it inhibits polar FtsZ ring formation [8, 9] and prevents minicelling.

Several deterministic [10, 11, 12, 13, 14] and stochastic models [15, 16, 17, 18, 19] have been developed to explain the pole-to-pole oscillation pattern of the Min proteins. All these quantitative models have recovered oscillatory behavior, though they differ in their detailed interactions.

The FtsZ ring is the first element of the divisome to localize [20]. Induced disassembly of the FtsZ ring can occur within a minute [21], and subsequent relocalization occurs within minutes. FtsZ can localize around potential division sites of daughter cells even before septation is complete [22]. Min oscillations must persist or be quickly regenerated after septation to ensure that polar FtsZ ring formation is blocked in newly formed daughters.

The experimental phenomenology of Min dynamics during septation has not yet been well characterized. Early experiments [7, 23] indicate that Min oscillations are qualitatively unaffected by partially constricted cells. Significantly, minicelling rates in wild-type *E. coli* cells are insignificant [24], and no non-oscillating daughter cells have been reported. These observations suggest that Min oscillations persist or regenerate quickly in all daughter cells and, as a result, block FtsZ ring formation at the poles of newly formed daughter cells.

In a pioneering study, Tostevin and Howard [19] addressed Min oscillations after cell division with a 1d stochastic model. Their model exhibited significant asymmetry in the distribution of Min proteins between the two daughter cells after division. Approximately 20% of their daughter cells did not oscillate due to such partitioning errors. While systematic studies of partitioning errors have not been done, large asymmetries of concentrations between daughter cells have not been reported. Tostevin and Howard suggested that rapid regeneration of Min proteins could quickly recover oscillations in non-oscillating daughters. However, no such cell-cycle dependent signal is seen in translation [25] or, for the *min* operon, in transcription [26]. Moreover, Min oscillations continue even when protein synthesis is stopped by chloramphenicol [5]. This indicates that proteolysis rates are small, so that fast unregulated turnover of Min proteins (independent of the cell-cycle) is also not expected.

In model systems, the MinD::MinE densities must be above a threshold or “stability boundary” for stable oscillations to be observed [14]. Experimentally, the position of the stability boundary is not precisely known though large overexpression of MinE does

lead to minicelling [27, 28]. We have explored how the distance of the parent cell from the stability boundary affects the partitioning and hence the percentage of daughter cells that oscillate. While *in vivo* quantification of Min concentration has been done [29], we have primarily varied the distance from the stability boundary by varying the concentration of Min proteins in the parent cell within a reasonable range. This has the advantage of keeping the stability boundary fixed. For completeness, we have also varied the model interaction parameters. These are generally under-determined by experiment — though diffusivities have now been measured *in vivo* [30].

In addition to varying existing parameters, we have also explored heterogeneous interactions along the bacterial length – following [18]. The different phospholipids that comprise the *E. coli* inner-membrane exhibit variable affinity for MinD [31]. Cardiolipin (CL) is preferentially localized to polar and septal membranes in *E. coli* [32, 33]. The differences in MinD affinity for anionic phospholipids like CL implies enhanced MinD binding to the poles and the growing septum. We explore the implications of this midcell and polar enhancement on Min partitioning after septation.

We study septation within the context of the model by Huang *et al.* [14], which is a deterministic, 3D model without explicit MinD polymerization. This model is significantly different from the stochastic, 1D, polymerizing model of Tostevin and Howard [19]. Strikingly, we find that our partitioning errors are comparable to those seen by Tostevin and Howard [19] despite the differences in the models. The model of Huang *et al.* still appears to be the best current model at recovering the Min oscillation phenomenology, though MinD polymerization appears to be called for experimentally [34] and has been used in several quantitative models of Min oscillation [17, 18, 19]. Our aim is to understand how asymmetric partitioning result from the dynamics of Min oscillations and explore possible ways of achieving adequate partitioning of Min between daughter cells. We analyze the origins of the partitioning error, and speculate about plausible partitioning mechanisms for Min proteins during the septation of *E. coli*.

2. Cell Division Model

The model developed by Huang *et al.* [14] includes many of the interactions observed experimentally [35, 36, 37, 38]:

$$\frac{\partial \rho_{D:ADP}}{\partial t} = D_D \nabla^2 \rho_{D:ADP} - \sigma_D^{ADP \rightarrow ATP} \rho_{D:ADP} + \delta_{mem} \sigma_{de} \rho_{de}, \quad (1)$$

$$\begin{aligned} \frac{\partial \rho_{D:ATP}}{\partial t} = & D_D \nabla^2 \rho_{D:ATP} + \sigma_D^{ADP \rightarrow ATP} \rho_{D:ADP} \\ & - \delta_{mem} [\sigma_D + \sigma_{dD} (\rho_d + \rho_{de})] \rho_{D:ATP}, \end{aligned} \quad (2)$$

$$\frac{\partial \rho_E}{\partial t} = D_E \nabla^2 \rho_E + \delta_{mem} \sigma_{de} \rho_{de} - \delta_{mem} \sigma_E \rho_d \rho_E, \quad (3)$$

$$\frac{\partial \rho_d}{\partial t} = - \sigma_E \rho_d \rho_E (M) + [\sigma_D + \sigma_{dD} (\rho_d + \rho_{de})] \rho_d \rho_E \quad (4)$$

$$\frac{\partial \rho_{de}}{\partial t} = - \sigma_{de} \rho_{de} + \sigma_E \rho_d \rho_E (M), \quad (5)$$

where ρ_{DADP} , ρ_{DATP} and ρ_E , are the cytoplasmic densities of MinD:ADP, MinD:ATP and MinE respectively and ρ_d , ρ_{de} are the densities of membrane-bound MinD and MinDE complex, respectively. The rates of binding of MinD:ATP to the bare membrane, the cooperative binding of MinD:ATP to membrane bound MinD:ATP, the binding of cytoplasmic MinE to membrane bound MinD:ATP, and the hydrolysis rate of MinD:ATP from the membrane under activation by MinE are given by σ_D , σ_{dD} , σ_E , and σ_{de} , respectively. The bacterium was modeled as a cylinder of length L and radius R , with longitudinal interval $dx = 0.0521$ and radial interval $dr = 0.0416$, and with poles represented by flat, circular end-caps. Lateral growth is significantly reduced during septation [39, 40], so we accordingly keep L constant. The density of cytoplasmic MinE at the membrane surface is $\rho_E(M)$, while $\delta_{mem} \equiv \delta(r - R) + \delta(z) + \delta(z - z_L) + \delta(z - L/2)\theta(r - r_s(t))$ limits reactions to the bacterial inner membrane. The last term denotes the growing septum at mid-cell, with $r_s(t) \in [0, R]$ being the radius of the circular open portion of the cylindrical cross-section at mid-cell. Diffusion is not allowed across the septum (for $r > r_s$), while membrane interactions take place independently on either side of the growing septum.

Pre-septation Min oscillations were allowed to stabilize in a cell with length $L = 5\mu m$ before the process of septation was initiated. Septation was initiated at 10 or more uniformly distributed phases of the Min oscillation period to determine the effect of this phase on the partitioning of Min proteins. Since the detailed septal closure dynamics of *E. coli* are not well constrained experimentally, we assume linear inward growth of the septum with the midcell septal radius given by

$$r_s(t) = R(1 - (t - t_s)/t_r), \quad t > t_s \quad (6)$$

where t_r is the duration of septation and t_s is the time at which septation starts. The area of the growing septum is then $A(t) = \pi(R^2 - r_s^2)$ for $t \in [t_s, t_s + t_r]$ ($A = 0$ for $t < t_s$ while $A = \pi R^2$ for $t > t_s + t_r$). This process of septal closure mimics the process of septal growth discussed by Burdett and Murray [1]. Since MinD:ATP has a greater affinity for anionic phospholipids such as CL [31, 41] and since CL domains are found to be localized around the cell poles and septal regions [32, 33], we also considered the case in which the rate of attachment of MinD:ATP (σ_D) was enhanced at the polar and septal membranes (by an amount σ_{Dmax}) compared to the attachment rate elsewhere on the curved surface of the cylindrical cell (σ_{D0}).

Fig. 1(a) and 1(b) show oscillations in the parent cell during the process of septation while Fig. 1(c) shows oscillations in both daughters after septation. A septation duration $t_r = 512$ seconds was chosen to be consistent with the proportion of septating cells observed in culture [42]. Significantly faster septation ($t_r = 350$ s) does not affect our results.

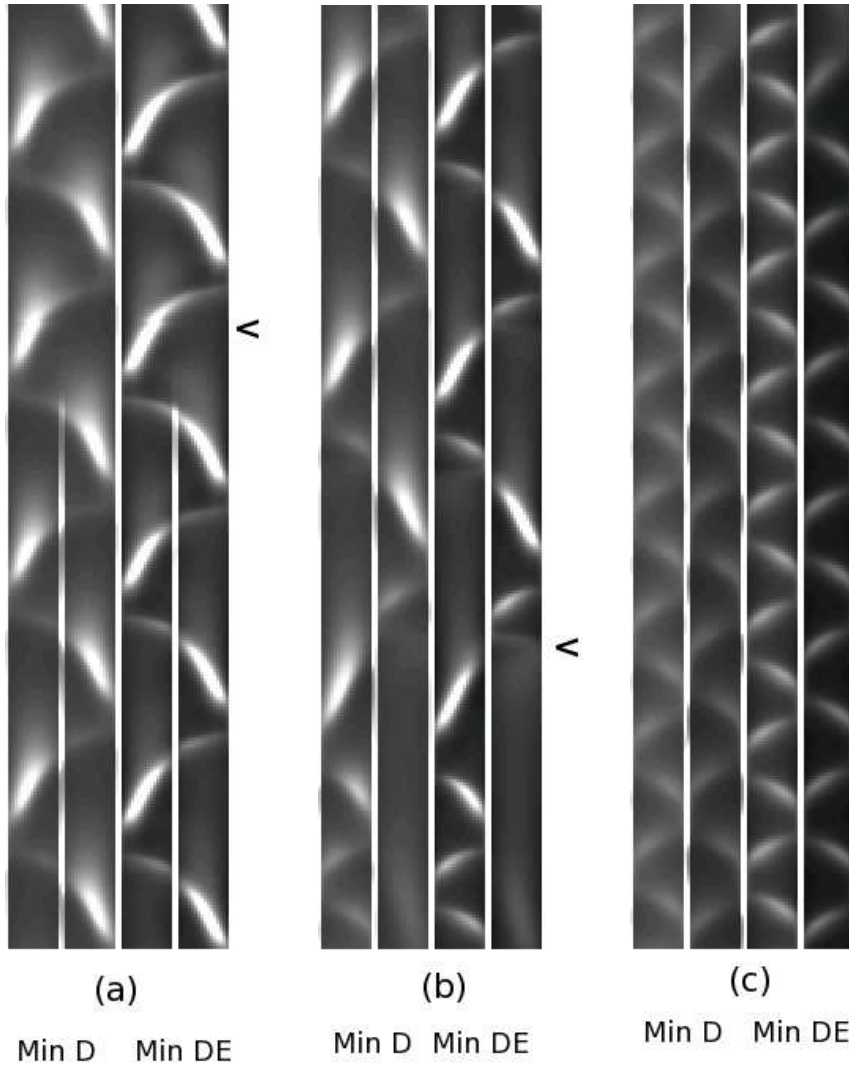


Figure 1. The time-development of membrane-bound MinD and MinDE during and after septation, represented as space-time plots. White and black indicate high and low linear densities, respectively. Time increases from top to bottom (total duration of 300 s is shown) while the bacterial length runs from left to right ($L = 5\mu m$) for each of MinD and MinDE. (a) Oscillations in parent cell starting from 100 s before and ending 200 s after septation. Membrane-bound MinD and MinDE are shown in the first and second columns respectively, as indicated. The arrowhead marks the beginning of the septation process and emerging white bar at midcell corresponds to the growing septum. (b) Oscillations just before and after the end of septation. The arrowhead marks the end of the septation process and formation of two independent daughter cells. Oscillations continue in the left daughter cell through septation but are disrupted and then regenerated in the right daughter cell after septation is complete. (c) Oscillations in both daughters after completion of septation. A significant asymmetry of Min partitioning between the two daughter cells is apparent. The parameters used in this figure are $\rho_D = 1150\mu m^{-1}$, $\rho_E = 350\mu m^{-1}$, $D_D = D_E = 2.5\mu m^2/sec$, $\sigma_{D0} = 0.025\mu m/sec$, $\sigma_{dD} = 0.0015\mu m^3/sec$, $\sigma_{de} = 0.7/sec$, $\sigma_E = 0.093\mu m^3/sec$, $\sigma_{Dmax} = 0.1\mu m/sec$. The three subfigures are contiguous in time.

3. Results

3.1. Varying Min concentration

We examined the effect of varying the MinD and MinE densities in the parent cell on the partitioning of Min between daughter cells. For this purpose, we generated 420 sets of different parent cell densities (ρ_D, ρ_E) . For each set, the initiation time of septation t_s was varied uniformly over the oscillation period T of the parent cell with at least 10 different phases sampled for each parent cell. Min partitioning information was noted at the end of the septation, and the simulation was run for more than 15 minutes after the end of septation to see whether Min oscillations were regenerated in the daughter cells.

Fig. 2 shows the linear density of MinD and MinE in parent cells (open triangles). Daughter cells with a variety of phases of septation start times are shown (smaller black and grey filled circles) for two representative parent cells (larger black and grey filled circles) close to and far from the stability boundary (approximately indicated by the black line), respectively. For oscillations to restart or continue in daughter cells, the ratio of MinD:MinE must be greater than ≈ 2.7 . Inadequate partitioning of Min results in daughter cells (\times) having Min densities which fall below this threshold. The partitioning for the pole-to-pole oscillating MinD is worse than for the more midcell MinE, resulting in an asymmetric donut-shaped distribution of daughter cell densities for a given parent cell. Since the MinE ring closely follows the MinD cap there is a correlation between the MinD and MinE partitioning — extending the asymmetric donuts along the diagonal. For parent cell densities close to the oscillation threshold, a large fraction of daughter cells do not oscillate. Away from the threshold a smaller fraction do not oscillate. Varying the duration of septation by moderate amounts does not change the partitioning, as illustrated by the nearly identical donuts for $t_r = 350s$ (open stars) and $t_r = 512s$ (black circles).

In Fig. 3(a) we show all of the partitioning donuts on one plot, where d_f and e_f are the fraction of MinD and MinE in the two daughter cells, respectively. The absence of any daughter cells in the central region, near $d_f = e_f = 0.5$, shows that simultaneous equipartitioning of both MinD and MinE is never observed. While there is always a septation start-time t_s , relative to the parent cell oscillation, that leads to perfect partitioning of MinD *or* MinE, there is no phase that leads to perfect partitioning of *both* MinD and MinE. This “donut hole” is a manifestation of the phase lag between MinD and MinE oscillations, i.e. the timing of maximal MinD at midcell is ahead of the timing of maximal MinE. To make this clear, in Fig. 3(b) we have scaled all of the partitioning donuts by their RMS radius, $r_{av} \equiv \sqrt{\langle (d_f - 0.5)^2 + (e_f - 0.5)^2 \rangle}$, and plotted the scaled densities $d_s \equiv (d_f - 0.5)/r_{av}$ vs. $e_s \equiv (e_f - 0.5)/r_{av}$. Relative to r_{av} , there are no phases that approach symmetric partitioning of both MinD and MinE.

We also plotted r_{av} against the oscillation period T of the parent cell in Fig. 4 to determine if the RMS radius scales with the period of oscillation of the parent cell. We do not see perfect collapse but r_{av} increases with period away from the stability

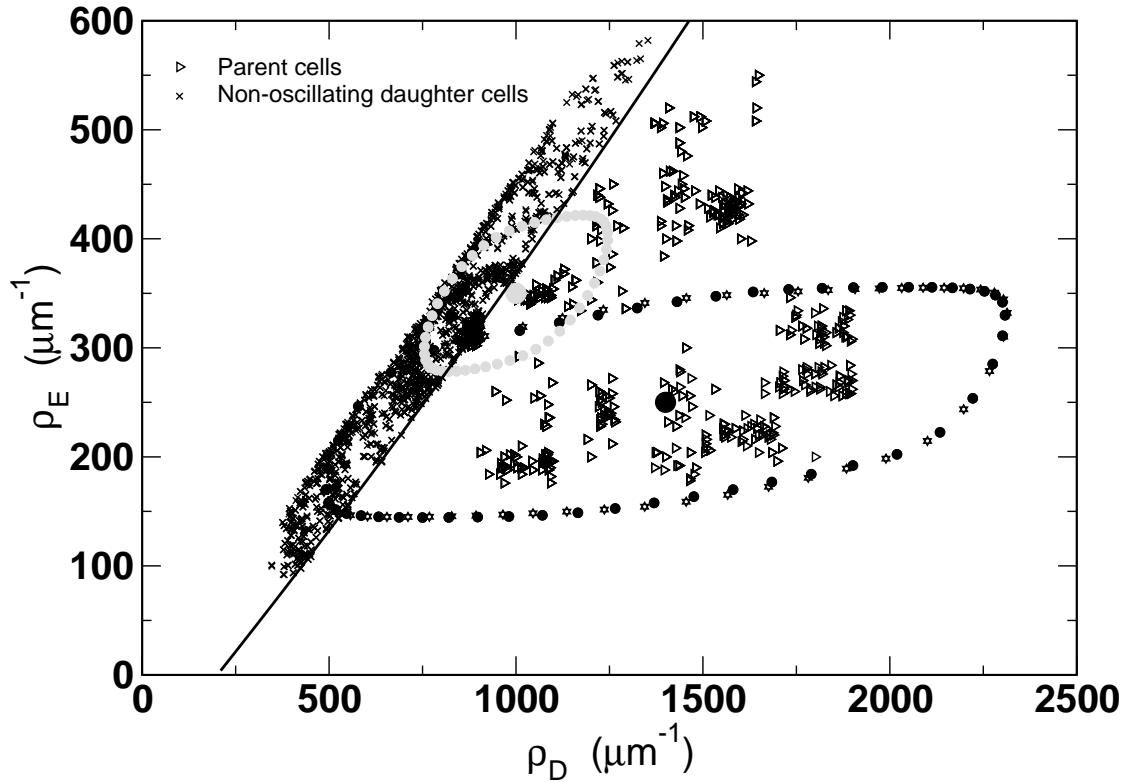


Figure 2. Scatter plot of linear MinD and MinE densities in the parent cell (open triangles) and non-oscillating daughter cells (\times). Indicated by the solid line is the approximate stability curve for $L = 5\mu\text{m}$ cells, separating oscillating and non-oscillating daughter cells. The large black and grey filled circles indicate example parent cells that lead to 84% and 58% oscillating daughter cells respectively. The smaller black and grey filled circles denote the corresponding linear densities of daughter cells produced after cell division. The open stars correspond to the black filled circle but with a septation duration of $t_r = 350$ seconds, all other points correspond to $t_r = 512$ seconds. Parameters are as specified in Fig. 1, but with $\sigma_{Dmax} = 0$.

boundary, indicating that the two partitioning donuts (formed by the small black or grey filled circles) shown in Fig. 2 are representative.

3.2. Enhanced MinD binding at poles and septum

To see whether a distinct phospholipid composition of the closing septum could affect the partitioning, we enhanced MinD:ATP binding (σ_D) at the cell poles and the growing mid-cell septum. The degree of enhancement was constrained by the practical requirement that it did not disrupt steady oscillations in the parent cell before t_s . This restricted the polar enhancement σ_{Dmax} to less than ten times the base value of $\sigma_{D0} = 0.025\mu\text{m}/\text{sec}$. This is consistent with the affinity of MinD:ATP for anionic

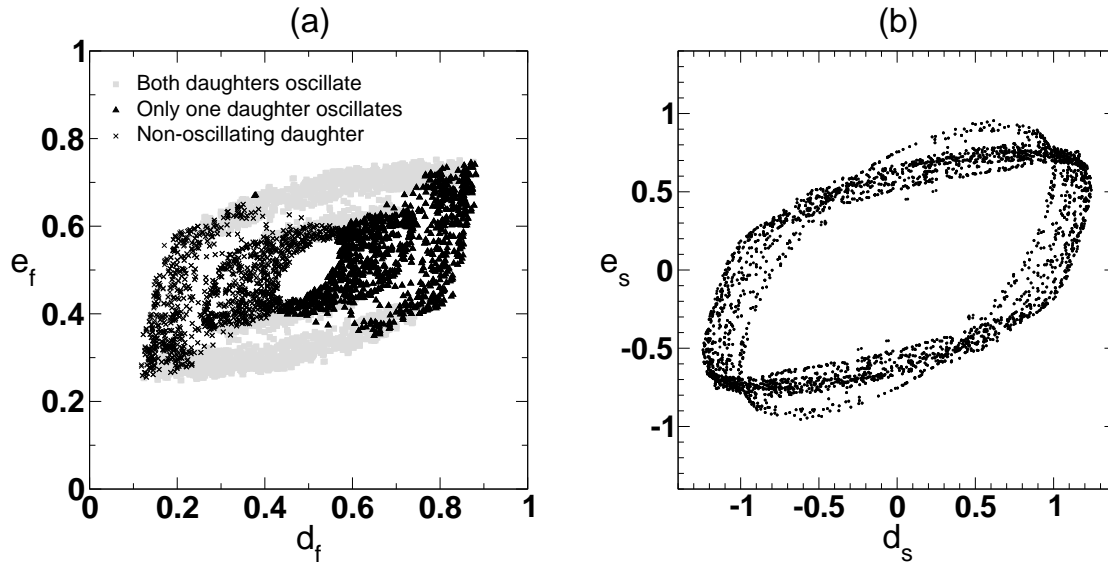


Figure 3. (a) Fractions, d_f vs. e_f of MinD and MinE, respectively, in oscillating as well as nonoscillating daughters for all parent cells. Black \times indicates non-oscillating daughter cells, while grey filled circles indicate oscillating daughter cells in cases where both daughter oscillates. Filled upper triangles correspond to fractions in the oscillating daughter for cases where only one daughter oscillates. The two daughter cells of a given parent are symmetrically placed around $d_f = e_f = 0.5$. (b) A plot of the scaled relative fractions of MinD vs. MinE in the two daughter cells.

phospholipids like cardiolipin, which is nine times higher than its affinity for zwitterionic phospholipids [32]. The enhancement of MinD:ATP binding at the poles and septum slightly increased the oscillation period in the parent cell by increasing the time for dissociation of membrane-bound MinD:ATP by MinE.

To analyze the effect of enhanced MinD binding at the poles and growing septum on the number of oscillating daughters, we compared the results from 50 parameter sets with and without septal and polar enhancement. In this comparison, the concentrations of MinD and MinE were varied while all other parameters were kept fixed and $\sigma_{Dmax} = 0.1\mu m/sec$ or $\sigma_{Dmax} = \sigma_{D0}$. The overall percentage of oscillating daughter cells increased by a small amount (2%) when enhanced polar and septal MinD:ATP attachment rates were used. More specifically, for parent cell density close to the stability threshold (large grey filled circle in Fig. 2), the enhancement of MinD:ATP binding at the poles and septum led to a modest increase (at most 2%) in the number of daughters which restart oscillations after septation. However, for parent cell densities far from the stability threshold (large black filled circle in Fig. 2) no significant increase in the number of oscillating daughters was obtained with enhanced MinD:ATP binding at the poles and growing septum.

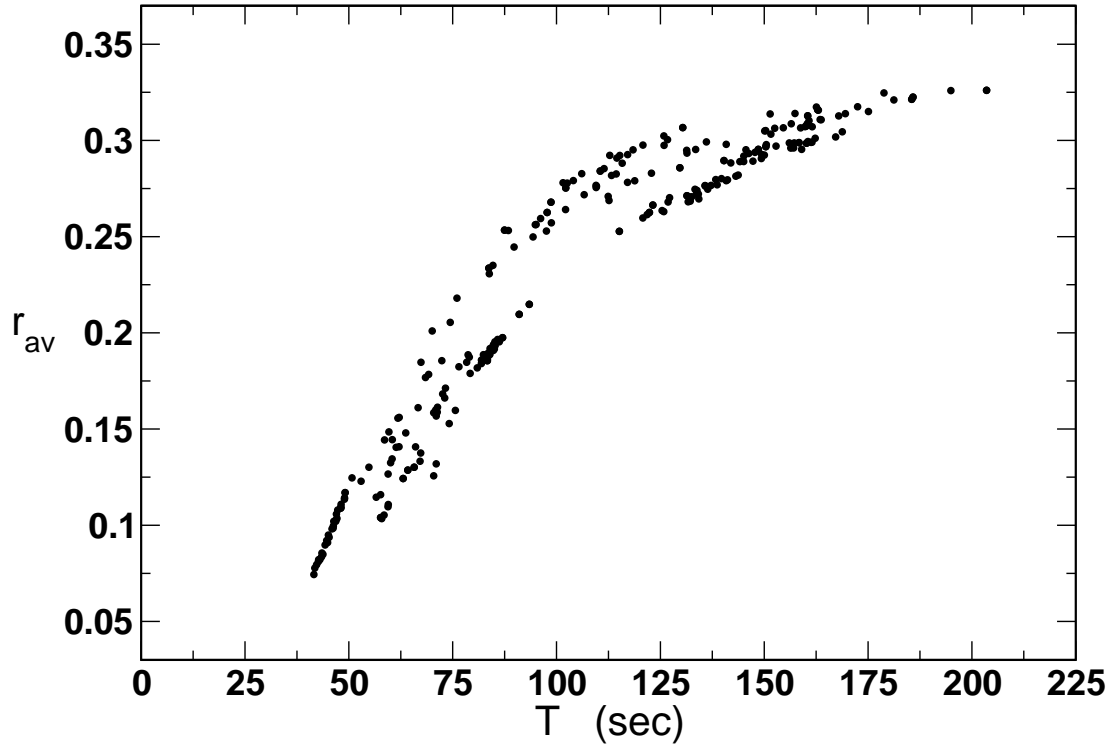


Figure 4. The RMS magnitude of partitioning error r_{av} vs. the oscillation period of the mother cell T . The period increases as the mother cell Min concentrations are moved away from the stability boundary shown in Fig. 2. While there is no precise scaling collapse, the trend is for less accurate partitioning as distance from the stability boundary (and hence T) increases — maintaining the non-oscillating daughters shown in Fig. 2. We do not find a significant dependence of r_{av} on the septation duration t_r .

3.3. Varying interaction parameters

In another attempt to increase the fraction of oscillating daughter cells after septation, we explored the parameter space of interactions in the Huang *et al.* model [14]. Since most of the parameters are experimentally under-determined, some flexibility is possible in the choice of parameters while insisting upon stable oscillations. In this context, the Min concentration, diffusivities, reaction rates, and σ_{Dmax} were all independently varied over plausible ranges for a fixed cell length. The parameter space was explored to move towards symmetric partitioning of MinD and MinE in non-oscillating daughter cells. Each parameter was varied over a range spanning almost an order of magnitude relative to the benchmark values which were chosen to be the parameters specified in Huang *et al.* However, no improvement upon the best 85% figure (obtained with or without polar and septal enhancement of the MinD binding rate) was obtained.

3.4. Phase dependence of partitioning

Why do we never see 100% of the daughter cells oscillating? The pattern of end-to-end oscillation of MinD continues largely unchanged throughout septation (see, e.g., Fig. 1), even as the period lengthens somewhat, so that when the *closure* of the septum coincides with MinD being localized predominately at one pole then the MinD will be badly partitioned between the two daughter cells. In Fig. 5 we plot the longitudinal position of the radially integrated MinD and MinE peaks away from the cell poles at the end of septation when $t = t_s + t_r$. Fig. 5(a) shows parent cells that lead to two oscillating daughters, while Fig. 5(b) shows parent cells that lead to only one oscillating daughter. We see that two oscillating daughters typically result from septation events where both MinD and MinE have a substantial peak at the mid-cell. When two oscillating daughters result despite polar maxima of MinD and MinE, a substantial midcell accumulation of MinD is also present. A non-oscillating daughter cell is typically produced when MinD has a large peak near one pole.

Fig. 6 illustrates the spatial profile of radially integrated MinD and MinE for three different phases at the end of septation. Fig. 6(a) corresponds to a phase where oscillation restarts in both daughters after septation. Adequate partitioning is reflected in large peaks of radially integrated MinD (solid line) and MinE (dashed line) near the midpoint of the cell. Fig. 6(b) corresponds to a phase where inadequate partitioning is manifest in the large peaks of radially integrated MinD (solid line) and MinE (dashed line) near one pole of the cell. Only one oscillating daughter results. Fig. 6(c) shows a peak in the radially integrated MinD and MinE near the midcell and pole respectively. The resulting inadequate partitioning of MinE between the two daughters ensures that the ratio of MinD:MinE falls below the threshold required to regenerate oscillations in one of the daughters. This leads to a non-oscillating daughter and corresponds to the points with a large midcell MinD peak in Fig. 5(b).

4. Discussion and Conclusions

We have explored the impact of MinD and MinE concentration, interaction parameters, and end-cap and septal cardiolipin patches on the partitioning of Min proteins between daughter cells after septation in the model of Huang *et al.* [14]. While concentration close to the stability threshold for oscillations led to less than 50% of daughter cells oscillating after septation, no combination of concentration, interaction parameters, and/or cardiolipin patches led to more than $\approx 85\%$ of daughter cells oscillating after septation. These results are comparable to those of Tostevin and Howard [19], despite significant differences in the Min models that were used. They studied a stochastic one-dimensional model with explicit MinD polymerization, while we used a deterministic three-dimensional model without filamentous MinD structures. We do not expect that the inclusion of stochastic effects would significantly change our results, following [16].

We found that plotting the MinD vs. MinE densities in the daughter cells leads to

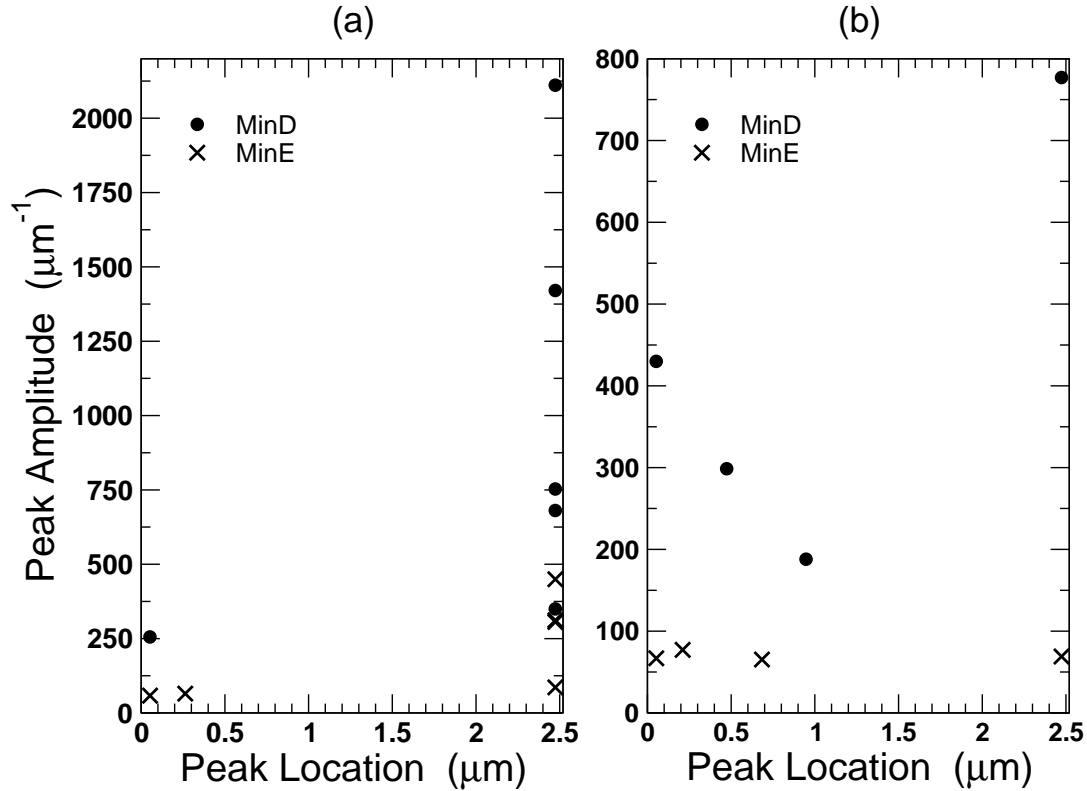


Figure 5. Non-polar “lateral” peak location of radially integrated MinD and MinE at the end of septation for phases which lead to (a) two oscillating daughters and (b) one oscillating daughter. Oscillations are observed in both daughters for 12 out of the 20 septating phases. Only half the cell length is plotted since the peak locations for different septating phases are symmetric about the mid-cell. In general, two-oscillating daughters result from a strong central peak of MinD at the completion of septation while one-oscillating daughter results from polar peaks, and hence weak and non-central lateral peaks. Parameters are as specified in Fig. 1, except for $\rho_D = 1400\mu m^{-1}$, $\rho_E = 250\mu m^{-1}$, $t_r = 512$ seconds, and $\sigma_{Dmax} = 0$.

a donut structure around the parent cell densities, and that varying the phase of the septal closure with respect to the end-to-end Min oscillation of the parent cell leads to daughter Min densities varying around the donut. The “missing hole” of the donut, i.e. the absence of daughter cells with the same Min densities as the parent cell, arises from the phase-difference between the leading MinD cap-forming and lagging MinE ring-forming oscillations. Furthermore, we find that there is always a phase of septation timing that leads to non-oscillating daughters. We believe that this is a fundamental aspect of end-to-end Min oscillation: when the MinD cap is at one pole, the distal pole is stable. This should be a generic feature of all Min oscillation models. The robustness of the best percentage of oscillating daughters under changes in concentration, parameter variation, heterogeneous perturbations, model variation, dimensionality, and stochastic

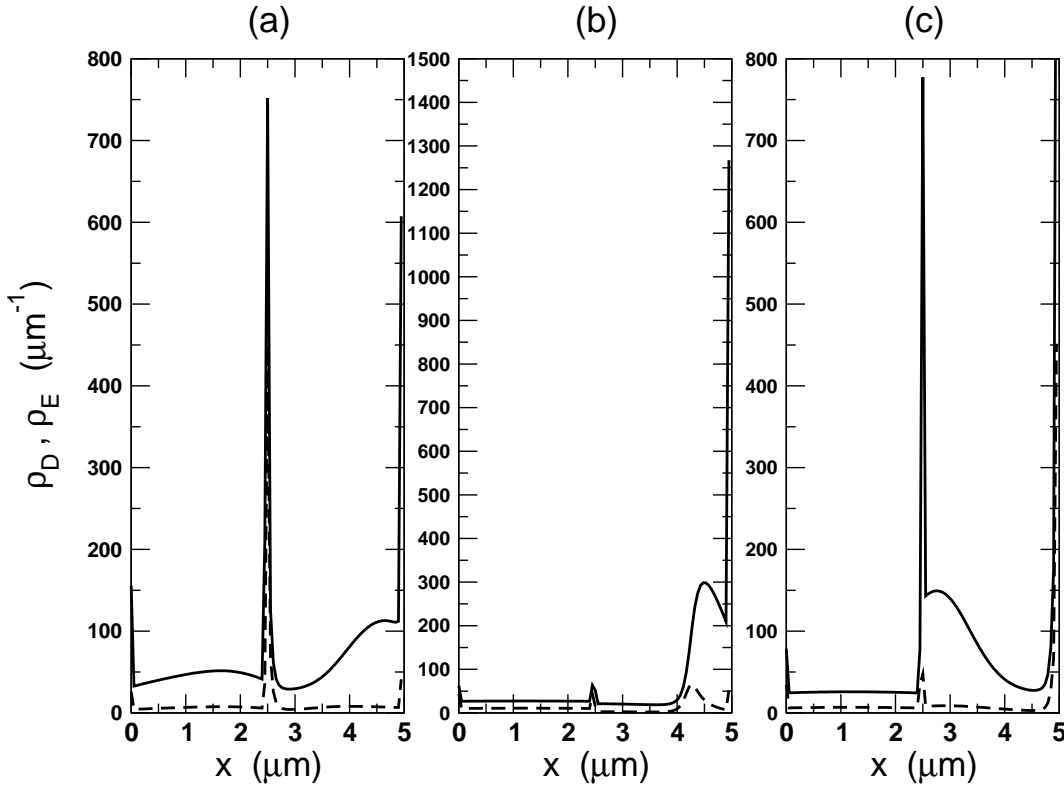


Figure 6. Profile along the cell length x of radially integrated (linear) densities of MinD (solid line) and MinE (dashed line) for three different phases of septation, at the time of septal closure. (a) leads to two oscillating daughter cells and exhibits strong central MinD and MinE peaks, (b) leads to only one oscillating daughter cell and exhibits a strong polar peak of both MinD and MinE, and (c) leads to only one oscillating daughter cell and exhibits a strong polar peak of MinE. The parameters used are the same as in the previous figure.

effects support this conclusion.

How might *E. coli* achieve its (observed) negligible level of minicelling? We see four basic possibilities.

As suggested by Tostevin and Howard [19], the non-oscillating daughters could be rescued by rapid regeneration of Min concentration. This would require Min synthesis to be regulated in a cell-cycle dependent manner. Because the average concentration of the two daughter cells equals their parent cell, rapid synthesis leading to recovery in one daughter cell would lead to a spike in Min concentration right after septation. However, there is no evidence of such fine-tuned regulatory control, or cell-cycle dependence, of Min concentration [25, 26]. Moreover, lack of adequate partitioning would give rise to substantial asymmetry of Min proteins in the two daughter cells that should be apparent in experimental studies — especially with the simple inducible promoters (not actively

regulated) typically used in Min-GFP fusion studies [5, 6, 7, 23, 29, 30, 34, 35]. In our simulations we found that the fraction of the parent MinD and MinE in daughter cells can be as low 15% and 25% respectively. The lack of any reports of such large visible asymmetries argues against rapid Min regeneration.

The partitioning problem can be avoided if the Min oscillations “double-up” before septation, leading to two symmetric oscillations in the two halves of the parent cell. A closing septum would then maintain symmetric Min distributions in the daughter cells. Indeed, we were hoping to promote this effect with the introduction of cardiolipin patches at poles and septum — without success. While there has been one experimental report of a doubling of oscillation for deeply constricted cells [7], this must be approached with caution due to the difficulty of distinguishing partial from full septation. We never found any evidence for doubling up of oscillations in our simulations. In all cases, we found that oscillations continue until just before the end of septation. Indeed, the Min oscillation wavelength of $\approx 8\mu\text{m}$ seen in filamentous cells [5] would suggest that it is difficult to spontaneously generate $L = 2\mu\text{m}$ oscillations while significant connection between the two ends of the parent cell remains.

Distortion and/or disruption of the Min oscillation by the growing septum before septal closure might also lead to symmetric partitioning of Min between the daughter cells. We do find that MinD binding to the sides of the growing septum improves partitioning. This was evident by comparing the partitioning for a finite septation time ($t_r = 512$ seconds) with instantaneous septation ($t_r = 0$). In the latter case, no MinD can accumulate on the septum before the daughter cells are separated. This resulted in highly skewed Min distributions between the two daughter cells (results not shown). However, significant partitioning errors still occur with gradual septal growth. Moreover, no significant improvement in partitioning was observed when the MinD binding was enhanced at the midcell. We also found that Min oscillation was often temporarily disrupted in one daughter cell despite acceptable partitioning for oscillation in both daughters. The time required for recovery of steady oscillations was sometimes as large as 15 minutes. This is much larger than the dynamical time-scale of FtsZ rings [22], though, as shown by Tostevin and Howard [19], stochastic effects may eliminate or significantly decrease the regeneration time of oscillations. Disruption of the Min oscillation in both daughter cells by the late stages of septation may therefore be a viable partitioning mechanism *in vivo* especially if the resulting uniform distribution of Min is sufficient to block septation [43] in the face of fast FtsZ dynamics [22] while the Min oscillation is being regenerated. However, in our model we did not observe disruption in both daughter cells even with enhanced MinD binding at the growing septum.

Finally, the cell may coordinate the septal closure with the Min oscillation. As seen in Fig. 1 there are a number of phases where *both* daughter cells oscillate after septation. As shown in Fig. 5(a), and illustrated in Fig. 6(a), most of those phases correspond to midcell MinD and MinE peaks. Triggered septal closure that occurs only at these phases would always recover Min oscillation in both daughters. Such triggered

septal closure could result from the participation of the C-terminal domain of MinC in FtsZ ring *disassembly* towards the end of of septation [44]. Since septation occurs in Δmin mutants [43], any such effect would have to accelerate septation rather than cause it. Narrow constrictions have been observed in cryoelectron tomography studies of *Caulobacter crescentus* [45], though too infrequently to indicate a significant septation pause. In *E. coli*, mutations of the N-terminal domain of FtsK lead to the stalling of septation at a very late stage with deep constrictions [46], leading to speculation about pores between the daughter cells before septal closure [47]. The triggered septal closure discussed here would only require a pause (or speed-up) of at most one half period of the Min oscillation that could be lifted (or imposed) by the MinC at midcell.

The challenge lies in understanding how Min oscillations can persist or be regenerated in both daughter cells after septation, in the face of partitioning errors due to the end-to-end oscillation of the Min proteins. Without one or more of the additional mechanisms discussed above, we expect significant partitioning errors, leading to non-oscillating daughters, in all Min models. Experimental characterization of the Min oscillations during and after septation, and quantitative assessment of Min partitioning between the daughter cells will be invaluable in sorting out which of these four partitioning mechanisms, or what combination of these four mechanisms, plays a role in *E. coli*. We believe that the last mechanism, of triggered septal closure, is most likely the dominant mechanism *in vivo*. Reproducing Fig. 3 from experimental images of newly septated cells should be straightforward if both MinD and MinE have distinct fluorescent tags (see, e.g. [29]). The average of each fluorescent signal of the two daughter cells can be used to independently scale the corresponding MinD or MinE signal, without the need for calibration even in the face of photo-bleaching. Non-regenerating mechanisms of partitioning, such as septal triggering, would lead to a “double-bar” pattern of MinD vs MinE densities in the daughter cells (looking like \square) rather than the connected donuts seen in Fig. 3.

Acknowledgments

We thank Benjamin Downing and Manfred Jericho for useful discussions. This work was supported by the Canadian Institute of Health Research.

Glossary

1d: one-dimensional

3d: three-dimensional

RMS: root-mean-square

CL: cardiolipin

References

- [1] Burdett I D and Murray R G 1974 Electron microscope study of septum formation in *Escherichia coli* strains B and B-r during synchronous growth. *J. Bacteriol.* **119** 1039-1056.
- [2] Woldringh C L, Mulder E, Valkenburg J A, Wientjes F B, Zaritsky A and Nanninga N 1990 Role of the nucleoid in the toporegulation of division. *Res. Microbiol.* **141** 39-49
- [3] Yu X C and Margolin W 1999 FtsZ ring clusters in Min and partition mutants: role of both the Min system and the nucleoid in regulating FtsZ ring localization. *Mol. Microbiol.* **32** 315-326
- [4] Bernhardt T G and de Boer P A J 2005 SlmA, a nucleoid-associated FtsZ binding protein required for blocking septal ring assembly over chromosomes in *E. coli*. *Mol. Cell.* **18** 555-564
- [5] Raskin D M and de Boer P A J 1999 Rapid pole-to-pole oscillation of a protein required for directing division to the middle of *Escherichia coli*. *Proc. Nat. Acad. Sci. USA* **96** 4971-4976
- [6] Hale C A, Meinhardt H and de Boer P A J 2001 Dynamic localization cycle of the cell division regulator MinE in *Escherichia coli*. *EMBO J.* **20** 1563-1572
- [7] Hu Z and Lutkenhaus J 1999 Topological regulation of cell division in *Escherichia coli* involves rapid pole to pole oscillation of the division inhibitor MinC under the control of MinD and MinE. *Mol. Microbiol.* **34** 82-90
- [8] Huang J, Cao C and Lutkenhaus J 1996 Interaction between FtsZ and inhibitors of cell division *J. Bacteriol.* **178** 5080-5085
- [9] Hu Z, Mukherjee A, Pichoff S and Lutkenhaus J 1999 The MinC component of the division site selection system in *Escherichia coli* interacts with FtsZ to prevent polymerization *Proc. Nat. Acad. Sci. USA.* **96** 14819-14824
- [10] Meinhardt H and de Boer P A J 2001 Pattern formation in *Escherichia coli*: A model for the pole-to-pole oscillations of Min proteins and the localization of the division site. *Proc. Nat. Acad. Sci. USA* **98** 14202-14207
- [11] Howard M, Rutenberg A D and de Vet S 2001 Dynamic compartmentalization of bacteria: accurate division in *E. coli*. *Phys. Rev. Lett.* **87** 278102
- [12] Kruse K 2002 A Dynamic model for determining the middle of *Escherichia coli*. *Biophys. J.* **82** 618-627
- [13] Meacci G and Kruse K 2005 Min-oscillations in *Escherichia coli* induced by interactions of membrane-bound proteins. *Phys. Biol.* **2** 89-97
- [14] Huang K C, Meir Y and Wingreen N S 2003 Dynamic structures in *Escherichia coli*: Spontaneous formation of MinE rings and MinD polar zones. *Proc. Nat. Acad. Sci. USA* **100** 12724-12728
- [15] Howard M and Rutenberg A D 2003 Pattern formation inside bacteria: fluctuations due to the low copy number of proteins. *Phys. Rev. Lett.* **90** 128102
- [16] Kerr R A, Levine H, Sejnowski T J and Rappel W J 2006 Division accuracy in a stochastic model of Min oscillations in *E. coli*. *Proc. Nat. Acad. Sci. USA* **103** 347-352
- [17] Pavin N, Paljetak H Č and Krstić V 2005 Min oscillation in *Escherichia coli* with spontaneous formation of two-stranded filaments in 3D stochastic reaction-diffusion model *Phys. Rev.* **E 73** 021904
- [18] Drew D A, Osborn M J and Rothfield L I 2005 A polymerization-depolymerization model that accurately generates the self-sustained oscillatory system involved in bacterial division site placement. *Proc. Nat. Acad. Sci. USA* **102** 6114-6118
- [19] Tostevin F and Howard M 2006 A stochastic model of Min oscillations in *Escherichia coli* and Min protein segregation during cell division. *Phys. Biol.* **3** 1-12
- [20] Goehring N W and Beckwith J 2005 Diverse paths to midcell: Assembly of bacterial cell division machinery. *Curr. Biol.* **15** R514-R526
- [21] Addinall S G, Cao C and Lutkenhaus J 1997 Temperature shift experiments with an FtsZ84(Ts) strain reveals rapid dynamics of FtsZ localization and indicate that the Z ring is required throughout septation and cannot reoccupy division sites once constriction has initiated. *J. Bacteriol.* **179** 4277-4284

- [22] Sun Q and Margolin W 1998 FtsZ dynamics during the division cycle of live *Escherichia coli* cells. *J. Bacteriol.* **180** 2050–2056
- [23] Raskin D M and de Boer P A J 1999 MinDE-dependent pole-to-pole oscillation of division inhibitor MinC in *Escherichia coli*. *J. Bacteriol.* **181** 6419–6424
- [24] Frazer A C and Curtiss R 1975 Production, properties and utility of bacterial minicells. *Curr. Top. Micro. Immun.* **69** 1–84
- [25] Lutkenhaus J F, Moore B A, Masters M and Donachie W D 1979 Individual proteins are synthesized continuously through the *Escherichia coli* cell cycle. *J. Bacteriol.* **138** 352–360
- [26] Arends S J-Ryan and Weiss D s 2004 Inhibiting cell division in *Escherichia coli* has little if any effect on gene expression. *J. Bacteriol.* **186** 880–884
- [27] Pichoff S, Vollrath B, Touriol C, and Bouché J-P 1995 Deletion analysis of gene *minE* which encodes the topological specificity factor of cell division in *Escherichia coli* *Mol. Micro.* **18** 321–329
- [28] Zhao, C-R, de Boer, P A J, and Rothfield L I 1995 Proper placement of the *Escherichia coli* division site requires two functions that are associated with different domains of the MinE protein *Proc. Nat. Acad. Sci. (USA)* **92** 4313–4317
- [29] Shih Y L, Fu X, King G F, Le T and Rothfield L I 2002 Division site placement in *E. coli*: mutations that prevent formation of the MinE ring lead to loss of the normal midcell arrest of growth of polar MinD membrane domains *EMBO J.* **21** 3347–3357
- [30] Meacci G, Ries J, Fischer-Friedrich E, Kahya N, Schwille P, and Kruse K 2006 Mobility of Min-proteins in *Escherichia coli* measured by fluorescence correlation spectroscopy. *Phys. Biol.* **3** 255-263
- [31] Mileykovskaya E and Dowhan W 2000 Visualization of Phospholipid Domains in *Escherichia coli* by using the cardiolipin-specific fluorescent dye 10-N-Nonyl Acridine Orange. *J. Bacteriol.* **182** 1172–1175
- [32] Mileykovskaya E, Fishov I, Fu X, Corbin B D, Margolin W and Dowhan W 2003 Effects of phospholipid composition on MinD membrane interactions. *J. Bio. Chem.* **278** 22193–22198
- [33] Koppelman C M, den Blaauwen T, Duursma M C, Heeren R M and Nanninga N (2001) *Escherichia coli* minicell membranes are enriched in cardiolipin. *J. Bacteriol.* **183** 6144-6147
- [34] Shih Y L, Le T and Rothfield L 2003 Division site selection in *Escherichia coli* involves dynamic redistribution of Min proteins within coiled structures that extend between the two cell poles. *Proc. Nat. Acad. Sci. USA* **100** 7865–7870
- [35] Hu Z and Lutkenhaus J 2001 Topological Regulation of Cell division in *E. coli*: spatiotemporal oscillation of MinD requires stimulation of its ATPase by MinE and phospholipid. *Mol. Cell.* **7** 1337-1343
- [36] Hu Z, Gogol E P and Lutkenhaus J 2002 Dynamic assembly of MinD on phospholipid vesicles regulated by ATP and MinE. *Proc. Nat. Acad. Sci. USA* **99** 6761–6766
- [37] Suefuji K, Valluzzi R and RayChaudhuri D 2002 Dynamic assembly of MinD into filament bundles modulated by ATP, phospholipids, and MinE. *Proc. Nat. Acad. Sci. USA* **99** 16776–16781
- [38] Lackner L L, Raskin D M and de Boer P A J 2003 ATP-dependent interactions between *Escherichia coli* Min proteins and the phospholipid membrane in vitro. *J. Bacteriol.* **185** 735–749
- [39] Woldringh C L, Huls P, Pas E, Brakenhoff G J and Nanninga N 1987 Topography of peptidoglycan synthesis during elongation and polar cap formation in a cell division mutant of *Escherichia coli* MC4100. *J. Gen. Microbiol.* **133** 575–586.
- [40] Wientjes F B and Nanninga N 1989 Rate and topography of peptidoglycan synthesis during cell division in *Escherichia coli* : Concept of a leading edge. *J. Bacteriol.* **171** 3412–3419
- [41] Mileykovskaya E and Dowhan W 2005 Role of membrane lipids in bacterial division-site selection. *Curr. Opin. Microbiol.* **8** 135–142
- [42] Woldringh C L 1976 Morphological analysis of nuclear separation and cell division during the life cycle of *E. coli*. *J. Bacteriol.* **125** 248–257
- [43] de Boer P A J, Crossley R E, and Rothfield L I 1989 A division inhibitor and a topological specificity factor coded for by the minicell locus determine proper placement of the division

- septum in *E. coli* *Cell* **56** 641–649
- [44] Shiomi D and Margolin W 2007 The C-terminal domain of MinC inhibits assembly of the Z ring in *Escherichia coli*. *J. Bacteriol.* **189** 236-243
- [45] Judd E M, Comolli L R, Chen J C, Downing K H, Mowerner W E, McAdams H H 2005 Distinct constrictive processes, separated in time and space, divide *Caulobacter* inner and outer membranes *J. Bacteriol.* **187** 6874–6882
- [46] Begg K J, Dewar S J and Donachie W D 1995 A new *Escherichia coli* cell division gene, *ftsK*. *J. Bacteriol.* **177** 6211-6222
- [47] Donachie W D 2002 FtsK: Maxwell's demon? *Mol. Cell.* **9** 206-207